Kang, Running; An, Sufeng; Wang, Xuehai; Wang, Gang; Chen, Hong; Zhang, Cuijuan; Bin, Feng; Li, Yongdan

# Support effect and reaction pathway for NO direct decomposition over CuMn/A (A=ZSM-5, Beta, SSZ-13) catalysts

*Published in:*
Catalysis Today

*DOI:*
10.1016/j.cattod.2024.114545

Published: 15/03/2024

*Document Version*
Publisher's PDF, also known as Version of record

*Please cite the original version:*
Kang, R., An, S., Wang, X., Wang, G., Chen, H., Zhang, C., Bin, F., & Li, Y. (2024). Support effect and reaction pathway for NO direct decomposition over CuMn/A (A=ZSM-5, Beta, SSZ-13) catalysts. *Catalysis Today*, *430*, Article 114545. https://doi.org/10.1016/j.cattod.2024.114545

Catalysis Today 430 (2024) 114545

Contents lists available at ScienceDirect

Catalysis Today

journal homepage: www.elsevier.com/locate/cattod

# Support effect and reaction pathway for NO direct decomposition over CuMn/A (A=ZSM-5, Beta, SSZ-13) catalysts

Running Kang [a,b,c], Sufeng An [d], Xuehai Wang [d], Gang Wang [d], Hong Chen [e], Cuijuan Zhang [f], Feng Bin [b,c], Yongdan Li [a,*]

[a] Department of Chemical and Metallurgical Engineering, School of Chemical Engineering, Aalto University, Kemistintie 1, P.O. Box 16100, Espoo FI-00076, Finland
[b] State Key Laboratory of High-Temperature Gas Dynamics, Institute of Mechanics, Chinese Academy of Sciences, Beijing 100190, China
[c] School of Engineering Science, University of Chinese Academy of Sciences, Beijing 100049, China
[d] Dalian Research Institute of Petroleum and Petrochemicals, SINOPEC, Dalian 116045, China
[e] School of Environmental Science & Engineering, Tianjin University, Tianjin 300072, China
[f] Collaborative Innovation Center of Chemical Science and Engineering (Tianjin), Tianjin Key Laboratory of Applied Catalysis Science and Technology, State Key Laboratory of Chemical Engineering (Tianjin University), School of Chemical Engineering and Technology, Tianjin University, Tianjin 300072, China

ARTICLE INFO

*Keywords:*
NO direct decomposition
$CuMnO_x$
Zeolites
Support effect
Reaction pathway

ABSTRACT

The CuMn/ZSM-5 (CM/Z), CuMn/Beta (CM/B), and CuMn/SSZ-13 (CM/S) catalyst samples were prepared via an excess impregnation method to investigate the metal-support effect. The results show that the activity at 550 °C for NO direct decomposition follows the order of CM/Z (53.4%) > CM/B (49.2%) > CM/S (7.9%). The good activity and stability of CM/Z are attributed to a strong support effect including forming more active copper sites of the $(Cu^{2+}\text{-}O^{2-}\text{-}Cu^{2+})^{2+}$ and $(Cu^{+}\text{-}\square\text{-}Cu^{+})^{2+}$ dimers, which have higher redox activity, capacity of oxygen mobility, and NO sorption capability. The competitive adsorption between NO and $O_2$ on the oxygen vacancy of dimers over CM/Z results in the activity decrease from 53.4% to 40.3% at 550 °C after adding 1 vol% $O_2$. The reaction mechanism over CM/Z was discussed based on the in situ DRIFT and isotopic ($^{18}O_2$) experiments. Two NO adsorbs firstly on $(Cu^{+}\text{-}\square\text{-}Cu^{+})^{2+}$ to form $N_2O$, and $N_2O$ is activated to produce $N_2$, followed by the NO adsorption on $(Cu^{2+}\text{-}O^{2-}\text{-}Cu^{2+})^{2+}$ to form nitrite and nitrate species and decomposition to NO and $O_2$.

## 1. Introduction

The abatement of nitrogen oxides ($NO_x$) from the industrial exhaust gases remains a significant research task. The current technology, particularly selective catalytic reduction of $NO_x$ with ammonia ($NH_3$-SCR), has been successful as a commercial method to remove $NO_x$ in the flue gases [1–5]. However, the use of ammonia not only increases the operation cost for ammonia purchase and storage, but also causes second pollution of ammonia escape and catalyst deactivation via the ammonium sulfate formation [6,7]. Therefore, a great attention has been arisen in the scientific community to develop a direct $NO_x$ removing technique without any reductant with a suitable catalyst. The NO direct decomposition (NDD) into $N_2$ and $O_2$ has been regarded as the most effective solution to realize NO abatement [8–11]. However, as well known, the gaseous NO is so stable in gas phase that require a high temperature (>1000 °C) to break N-O bonding with an energy barrier of 364 kJ/mol. Overall, Compared with $NH_3$-SCR, the NDD is a simple de-$NO_x$ process with no secondary pollution but with a harsh condition of reaction and a high requirement of catalysts. Hence it is crucial to design an appropriate catalyst for NDD at suitable temperature.

The molecular sieve supported catalyst has been explored for NDD in recent years [12]. Particularly, ZSM-5 zeolite is regarded as a representative zeolite material to provide more active centers via ion exchange due to its high specific surface area and stable pore structure [13]. Meanwhile, the transition metal oxides (e.g. Cu, Ni and Fe oxides) acting as active sites are loaded on the zeolites because of their good adsorption and reduction ability [12]. Iwamoto and coworkers firstly found that copper ion-exchanged zeolites have activity for NDD, and further discovered that Cu-ZSM-5 exhibits better catalytic performance with NO conversion > 80% at 550 °C (W/F = 4.0 g·s·cm$^{-3}$, 1 vol% NO/He) [14,15]. Thereafter, many significant works were done to gain a deep understanding on the NDD mechanism, i.e. active sites and reaction pathways for the zeolite supported metal oxide catalysts. Recently, Wang et al. suggested that the transition of $Cu(OH)^{+}$ to $[Cu\text{-}O\text{-}Cu]^{2+}$

---

[*] Corresponding author.
*E-mail address:* yongdan.li@aalto.fi (Y. Li).

https://doi.org/10.1016/j.cattod.2024.114545
Received 23 November 2023; Received in revised form 28 December 2023; Accepted 19 January 2024
Available online 24 January 2024

dimer is accelerated with the increase of temperature, which promotes NO conversion over a Cu-ZSM-5 catalyst [16]. To explore the effect of promoters on the Cu-ZSM-5, Pârvulescu et al. prepared Cu-M-ZSM-5 catalysts (M=Ce, Sn, Tl) with a co-exchange method, and found that the introduction of the second metal leads to a better positioning of Cu and promotes the catalytic activity [17]. Liu et al. observed that the co-doping with Ni and La into Cu-ZSM-5 improved the activity for NDD and attributed to that the La doping effectively promotes the Cu species dispersion with formation of more $Cu^{2+}$ ions, while Ni facilitates $Cu^{2+}$ implantation to produce $(Cu^{2+}\text{-}O^{2\text{-}}\text{-}Cu^{2+})^{2+}$ dimers, verified by $O_2$-TPD and NO-TPD results [18]. In contrast, other researchers proposed via DFT results that a reduced $Cu^{+}\ldots Cu^{+}$ pair ($[Cu_2O]^{2+}$ active site) on Cu-ZSM-5 promotes NO adsorption and form $N_2O$ intermediates to decompose into $[Cu\text{-}O\text{-}Cu]^{2+}$ and $N_2$ [19,20]. In addition, there have been many investigations on the effect of zeolite (ZSM-5, SSZ-13, SAPO-34, etc.) in the $NH_3$-SCR reaction [21–24]. Lei et al. demonstrates direct experimental evidence for the dynamic redox cycling (i.e., $Cu^{II} \leftrightarrow Cu^{I}$) of Cu sites under zeolite confinement and provides new insights into the monomeric-to-dimeric Cu transformation for completing the Cu redox cycle over Cu-SSZ-13 in $NH_3$-SCR reaction [24]. However, the intrinsic active sites of the catalysts are under debate, and the reaction pathways including NO decomposition and competitive adsorption of $NO/O_2$ are still unclear for NDD reaction because of the absence of in situ experiments analysis.

In this work, the CuMn/A (A=ZSM-5, Beta, SSZ-13) catalyst samples are examined and the synergistic effect is explored. The good performance and detailed reaction mechanism of CuMn/ZSM-5 are deeply discussed based on the in-situ DRIFT and isotopic ($^{18}O_2$) transient exchange experiments together. The results elucidate the effect of different supports on the catalytic activity and the reaction pathways of NDD.

## 2. Experimental

### 2.1. Sample preparation

The samples were prepared with a conventional excess impregnation method. Prescribed amounts of $Cu(NO_3)_2\cdot 3\,H_2O$ and $Mn(NO_3)_2\cdot 4\,H_2O$ to keep the mole ratio of Cu and Mn as 1:1 were dissolved in distilled water. The solution was stirred continuously at 80 °C and immersed into the commercial zeolite as support (ZSM-5, Beta and SSZ-13) to achieve cation exchange with a loading of 6 wt% Cu and 5 wt% Mn. Afterwords, the material was dried at 120 °C overnight and calcined at 600 °C for 4 h. The obtained samples were named as CM/Z ($CuMnO_x$/ZSM-5), CM/B ($CuMnO_x$/Beta) and CM/S ($CuMnO_x$/SSZ-13), respectively. The actual loadings of copper and manganese in each catalyst were measured with X-ray fluorescence (XRF) analysis (Epsilon l Research and a Power 4200 scanning XRF spectrometer), as shown in Table 1, they are in good agreement with the prescription.

### 2.2. Characterization

The X-ray diffraction (XRD) patterns were acquired with a X`PERT PRO MPD Alpha1 diffractometer (40 mA, 45 kV) using Cu Kα radiation source. The specific surface area (SSA) was measured with BEL sorp Mini II instrument, and the $N_2$ adsorption isotherms were obtained at − 196 °C after outgassing pretreatment at 250 °C for 4 h. Scanning electron microscope (SEM, Hitachi S-4800) instrument equipped with an energy dispersive X -ray detector (EDX) mapping was used to measure the microstructures. The oxidation states of Cu, Mn and O species were recorded with an X-ray photoelectron spectroscopy (XPS, Kratos Axis Ultra DLD spectrometer). The XPS analysis was carried out under vacuum pressure ($\sim 5\times 10^{-8}$ Pa) at ambient temperature. The binding energy was calibrated with the C1s peak as internal standard (284.8 eV).

**Table 1**
The elemental contents of the samples.

| Sample | Mole ratio of Cu:Mn | Cu/wt% | Mn/wt% | Si/wt% | Al/wt% |
|---|---|---|---|---|---|
| CM/Z | 1:1 | 5.67 | 4.48 | 37.75 | 2.82 |
| CM/B | 1:1 | 5.88 | 4.90 | 36.19 | 2.69 |
| CM/S | 1:1 | 5.45 | 4.88 | 36.64 | 3.92 |

$H_2$ temperature-programmed reduction ($H_2$-TPR) and temperature-programmed desorption of $O_2$ ($O_2$-TPD) were done on ichem700 apparatus equipped with a thermal conductivity detector (TCD). Each sample was firstly pretreated at 500 °C for 1 h under Ar flow (30 mL/min) and cooled down to room temperature (RT). For $H_2$-TPR, 50 mg sample was heated at 10 °C/min from RT to 600 °C under 5 vol%$H_2$/Ar (30 mL/min) flow. In $O_2$-TPD experiment, 100 mg of sample was pre-adsorbed with $O_2$ (30 mL/min) for 1 h at RT, and then heated from RT to 950 °C at 10 °C/min with pure Ar (30 mL/min) flow after purging with pure Ar for 0.5 h. Temperature-programmed desorption of NO (NO-TPD) was measured with Mass spectrometer (MS, Pfeiffer Omnistar™) as the detector. The sample (200 mg) was adsorbed to saturation in 2 vol% NO/Ar for 1 h at 50 °C after pretreatment at 500 °C under Ar (30 mL/min) for 1 h. The desorbed gas signal was recorded with the MS from 50 °C to 600 °C at 10 °C/min in pure Ar flow.

*In situ* Diffuse reflectance infrared Fourier transform (DRIFT) spectroscopy (Thermo Fisher Scientific Nicolet iS50) experiments were performed to record the adsorbed species and intermediates during NDD reaction. The sample was pretreated with He (30 mL/min) at 500 °C, and the sample background spectra were collected at each temperature point in the cooling process. Afterwards, the feed was switched to mixed gas with 1 vol% NO/He, and/or 1 vol% NO+ 2 vol% $O_2$/He (30 mL/min) to adsorb and realize surface reaction at 30, 200, 300, 400, 500, 550 and 600 °C. Here, in order to explore the obvious effect of $O_2$ during NDD reaction, the mixed gas of 1 vol% NO + 2 vol% $O_2$ was applied to obtain detailed adsorbed species clearly. The steady spectra were collected at each temperature with 32 scans.

The steady isotopic labeling ($^{18}O_2$, from WUHAN NEWRADAR SPECIAL GAS Co., LTD.) experiments were done with switching instantaneously in an in situ fixed-bed reactor (i.d. = 3 mm), to trap transient response signals of reactants and products rapidly via online MS (Pfeiffer Omnistar™). To ensure steady operation and obtain transient response signal of reactants and products, four-way switch valve was successfully applied to switch the gas paths quickly and maintain continuous flow of reactant gases in our previous study [25]. The reactants include $N^{16}O$ ($m/z = 30$), $^{18}O_2$ ($m/z = 36$) and Ar ($m/z = 40$). The products contain $N_2$ ($m/z = 28$), $^{16}O_2/N^{18}O$($m/z = 32$), $^{16}O^{18}O$ ($m/z = 34$), $N_2^{16}O$($m/z = 44$), $N_2^{18}O/N^{16}O_2$ ($m/z = 46$), $N^{16}O^{18}O$ ($m/z = 48$), and $N^{18}O_2$($m/z = 50$). The sample (60 mg) was treated at 550 °C for 0.5 h in pure Ar. Then the 1 vol% NO/Ar (20 mL/min) was constantly fed into reactor at 550 °C for 15 min. Then the reactor was purged using pure Ar (30 mL/min) for 10 min. Premixed gas with 1 vol% NO + 1 vol% $^{18}O_2$/Ar (20 mL/min) was introduced at 550 °C for about 15 min to monitor the isotopic products adequately.

### 2.3. Catalytic activity

0.5 g catalyst sample (35–45 mesh) was put into a fix-bed quartz tube reactor (i.d. = 6 mm). All samples were pretreated to remove the gaseous impurities on the sample surface at 500 °C for 0.5 h in the Ar atmosphere (30 mL/min) and then cooled down to room temperature. The inlet gas with 8000 ppm NO/Ar was introduced into the reactor with a total flow rate of 30 mL/min (W/F=1 $g\cdot s/cm^3$). Each desired reaction temperature point was maintained for about 20 min to reach the steady state. A K-type thermocouple was located before the catalyst bed to measure the reaction temperature along the gases flow. The $N_2$ concentration was detected and quantified online using a MS (Pfeiffer Omnistar™) after calibration with internal standard method. The oxygen resistance of catalyst was measured with adding 1 vol% $O_2$ at 8000 ppm NO/Ar with a total flow rate of 30 mL/min. The TOF ($s^{-1}$) were calculated at a specified temperature of 450 °C in the kinetic regime.

The activity is evaluated with NO conversion to $N_2$ (NTN2) with equation (1),

$$NO \quad Conversion \quad to \quad N_2 = \frac{2[N_2]_{out}}{[NO]_{in}} \times 100\% \tag{1}$$

where $[NO]_{in}$ and $[N_2]_{out}$ are the inlet and outlet concentrations of NO and $N_2$, respectively.

$$\mathrm{TOF} = \frac{X \times C_o}{n} \tag{2}$$

Where X is NTN2 (%) at 450 °C, $C_0$ is the initial NO concentration with mol/s, and n (mol) is the molar mass of Cu and Mn in the catalysts, detected by XRF results.

## 3. Results

### 3.1. Catalytic performance

The catalytic activity of the catalyst samples in NDD were tested at different temperatures (Fig. 1). In Fig. 1(a), CM/Z and CM/B exhibit much higher activity than CM/S after 400 °C. Specifically, the NTN2 of CM/Z, CM/B and CM/S at 550 °C are 53.4%, 49.2% and 7.9%, respectively. The values of TOF decreased in the order of CM/Z ($4.73 \times 10^{-5}$ $s^{-1}$) > CM/B ($1.85 \times 10^{-5}$ $s^{-1}$) > CM/S ($1.16 \times 10^{-5}$ $s^{-1}$), in consistent with the sequence of activity results. With 1 vol% $O_2$, the activity decreases from 53.4% to 40.3% at 550 °C over CM/Z, indicating $O_2$ addition has an inhibition effect. The CM/Z maintains a good stability with 40% NTN2 over 8 h under the existence of 1 vol% $O_2$, see Fig. 1(b).

### 3.2. Structure and texture

As shown in Fig. 2, CM/Z, CM/B and CM/S display typical diffraction patterns of ZSM-5, Beta and SSZ-13 zeolite structures with high crystallinity, respectively [21,26,27]. In the 2θ range of 32–40, there are two weak peaks of CuO (JCPDS 80–1268) at 35.5° and 38.7°, and no visible $MnO_2$ diffraction peak for all the three samples, indicating that the CuO and $MnO_2$ are well dispersed on the surface of zeolite supports. The XRF results in Table 1 confirm that all catalysts exhibit almost identical contents of Cu and Mn. The calculated Si/Al ratios of CM/Z, CM/B and CM/S are 13.4, 13.5, and 9.3, respectively.

The $N_2$ adsorption-desorption curves and pore size distributions of the three samples are plotted in Fig. 3. All samples exhibit a strong interaction at low value of relative pressure ($P/P_0$), attributed to the strong adsorption potential occurred in micropores. The specific surface area (SSA) calculated by BET method of CM/Z, CM/B and CM/S are 330.6, 414.9 and 560.7 $m^2/g$, respectively. Moreover, the pore size distribution calculated by Barrett-Joyner-Halenda (BJH) method of CM/Z, CM/B and CM/S focus on < 1 nm, indicating that the catalysts are dominated with micropores (Fig. 3b).

The micrographs and element mapping of the samples are illustrated in Fig. 4. CM/Z exhibits regular and bright crystalline aggregates with distinct edges of typical ZSM-5 zeolite [28]. The homogeneous small spots on the CM/Z surface are attributed to the CuO and $MnO_2$ species. The CM/B presents aggregation of smaller particles (Fig. 4c), while CM/S shows bigger particles with layered surface of irregular cubes (Fig. 4e). Cu, Mn, and O elements all distribute uniformly on the catalyst surface, confirmed by the EDX mapping results in Fig. 4(b), (d) and (f).

### 3.3. Surface states and chemisorption

The Cu 2p spectra show two peaks at binding energies (BE) of ~955 and ~934.5 eV on the XPS curve of all the three samples (Fig. 5a), attributed to Cu $2p_{1/2}$ and $2p_{3/2}$, respectively [29]. The observed two satellite peaks at 941.5–944.5 eV suggest the existence of $Cu^{2+}$, and the satellite peak at 951.3 eV indicates the formation of $Cu^{+}$. Then Cu $2p_{3/2}$ peak is deconvoluted into two peaks at 934.5 and 931.7 eV, corresponding to $Cu^{2+}$ and $Cu^{+}$, respectively. The Mn 2p spectrum in Fig. 5(b) shows Mn $2p_{1/2}$ peak at 954.0 eV and Mn $2p_{3/2}$ peak at 642.0 eV. The Mn $2p_{3/2}$ can be deconvoluted into two peaks at 641.9 eV for $Mn^{3+}$ and 643.5 eV for $Mn^{4+}$ [30]. The lower BE peak in O 1 s spectra is assigned to the metal oxide species ($O_{lat1}$) and the higher BE is labeled as the lattice oxygen species ($O_{lat2}$) of the zeolite layers [31]. The element ratios of the samples are calculated by peak areas for semi-quantitative analysis, as listed in Table 2. The ratios of $Cu^{+}/Cu^{2+}$ (0.46) and $O_{lat1}/(O_{lat1}+O_{lat2})$ (0.16) are the highest on the CM/Z.

$H_2$-TPR was used to probe the reducibility of catalysts, as presented in Fig. 6(a). The two reduction peaks of all the samples center at around 251 and 345 °C, which are mainly attributed to the reduction of CuO clusters [32], and the reduction of isolated $Cu^{2+}$ [33], respectively. Obviously, CM/Z shows a high and sharp peak at low temperature (251 °C) for CuO clusters reduction, suggesting the surface CuO clusters are easily reduced via the $(Cu^{2+}\text{-}O^{2-}\text{-}Cu^{2+})^{2+}$ to $(Cu^{+}\text{-}[]\text{-}Cu^{+})^{2+}$ route, verified by the previous work [18]. In addition, the weak peak at 443 °C is assigned to the reduction of $Mn_2O_3$ to $Mn^{2+}$ [34]. The amount of $H_2$ consumption calculated in Fig. 6(d) follows the order of CM/Z (0.90 mmol/g) > CM/B (0.74 mmol/g) > CM/S (0.65 mmol/g).

$O_2$-TPD was applied to investigate the mobility of oxygen species in the samples. The observed $O_2$ desorption peaks in Fig. 6(b) can be classified into three parts. The desorption peak at about 66 °C in all catalysts is assigned to physically adsorbed oxygen. The chemically adsorbed oxygen species are usually formed on amorphous metal oxides

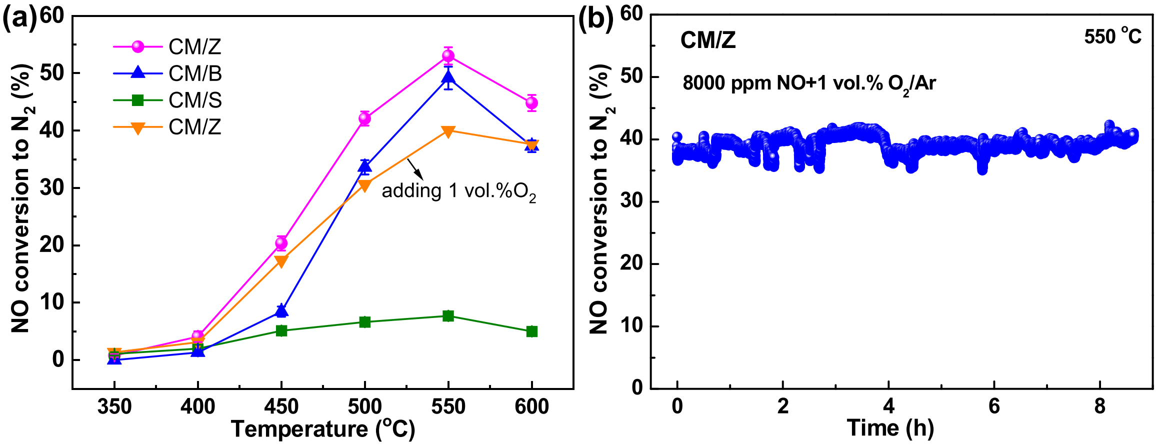

**Fig. 1.** (a) NO direct decomposition activity of CM/Z, CM/B and CM/S catalysts under 8000 ppm NO/Ar. (b) Long-term stability of CM/Z at 8000 ppm NO/Ar + 1 vol% $O_2$.

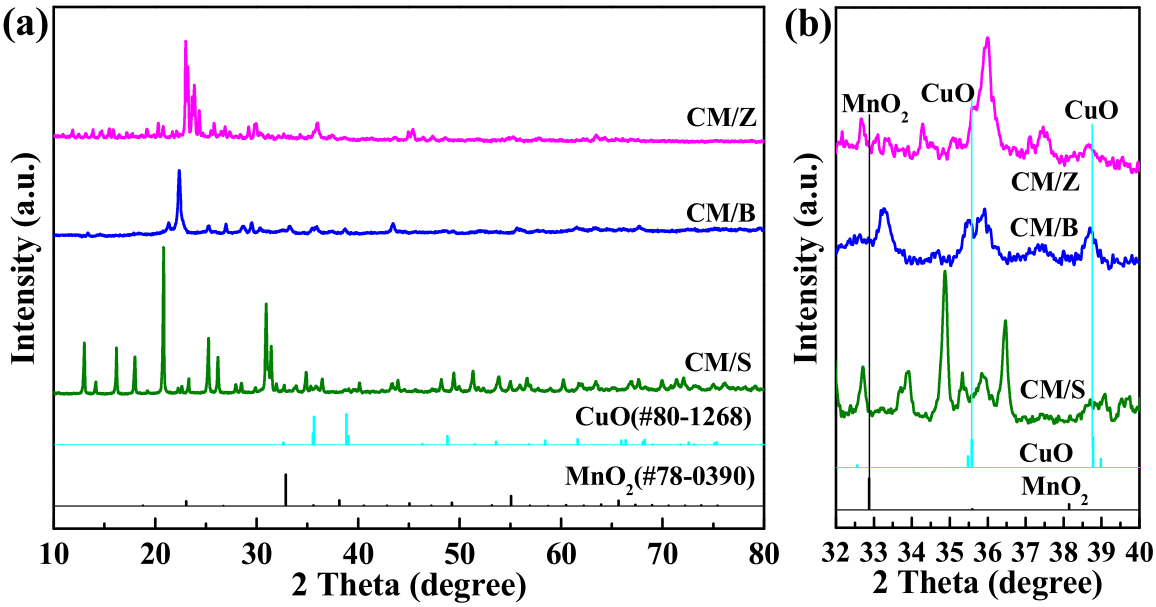

**Fig. 2.** (a) XRD patterns of samples and (b) the enlarged patterns in the range of 32–40°.

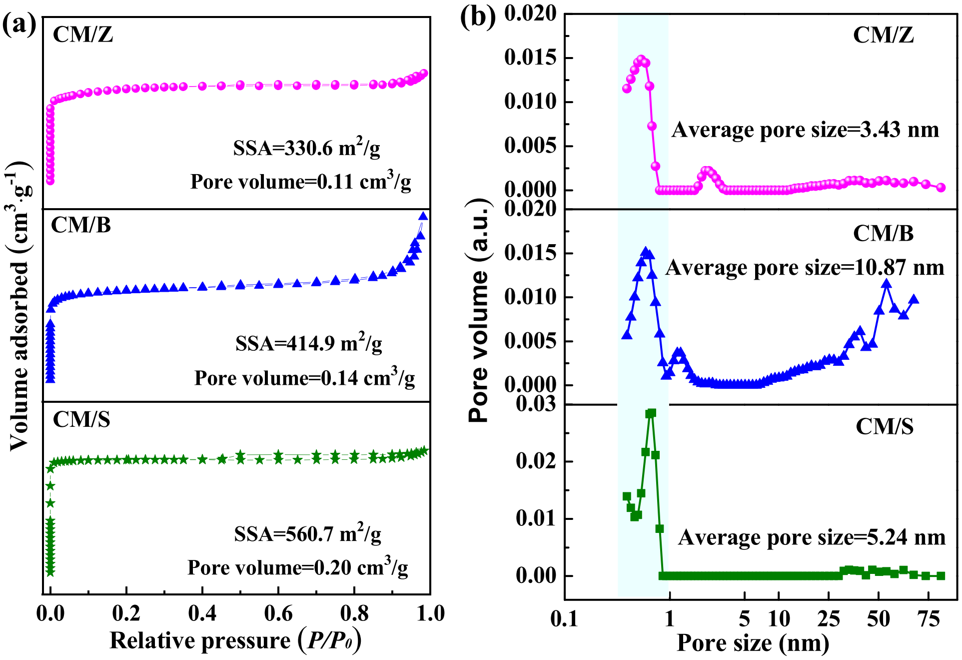

**Fig. 3.** (a) $N_2$ adsorption -desorption isotherms, and (b) pore size distribution curves of the CM/Z, CM/B and CM/S catalyst samples.

and/or surface oxygen vacancies on bulk metal oxides, corresponding to the desorption temperature at 279 °C for CM/B, 445 °C for CM/Z, and 477 °C for CM/S. The desorption peak at > 690 °C is related to the bulk lattice oxygen bonded to matrix metal ions [35]. CM/Z exhibits the largest desorption peak area of the chemisorbed oxygen and CM/S has a very small peak area. Hence, the capacity of oxygen mobility follows the sequence of CM/Z > CM/B > CM/S.

NO-TPD curves of the samples are illustrated in Fig. 6(c). The peak at around 125 °C is referred to the NO desorption from the $Cu^{2+}$ ions on the zeolite supports. The peaks centered at 304 °C and 463–480 °C are mainly attributed to the NO desorption on the $(Cu^{2+}\text{-}O^{2\text{-}}\text{-}Cu^{2+})^{2+}$ and $(Cu^{+}\text{-}\square\text{-}Cu^{+})^{2+}$ sites [36]. The CM/Z shows a bigger peak for NO desorption on the $(Cu^{+}\text{-}\square\text{-}Cu^{+})^{2+}$ meanwhile CM/S nearly does not have that peak due to the nonexistence of $Cu^{+}$, in good consistency with the XPS results. The CM/Z shows the highest NO adsorption capacity with the largest amount of NO adsorption (27.62 umol/g), benefitting to its catalytic activity. In summary, the $H_2$ consumption and NO adsorption of catalysts follows the CM/Z > CM/B > CM/S.

### 3.4. *In situ DRIFT and isotopic ($^{18}O_2$) tracing experiments*

*In situ* DRIFT spectra was measured to probe the reaction pathways of NDD with/without $O_2$ over CM/Z, as shown in Fig. 7. The bands at 2218 cm$^{-1}$ belong to the adsorbed $N_2O$ species [37]. The sharp peaks at 1900 and 1875 cm$^{-1}$ are assigned to the adsorbed NO on the $Cu^{2+}$ [37]. The 2133 and 1632 cm$^{-1}$ bands correspond to the ionic state of $NO_2^+$ and adsorption state of $NO_2$, respectively [38]. The different nitrate species of bridge coordination and unidentate species are formed at 1600 and

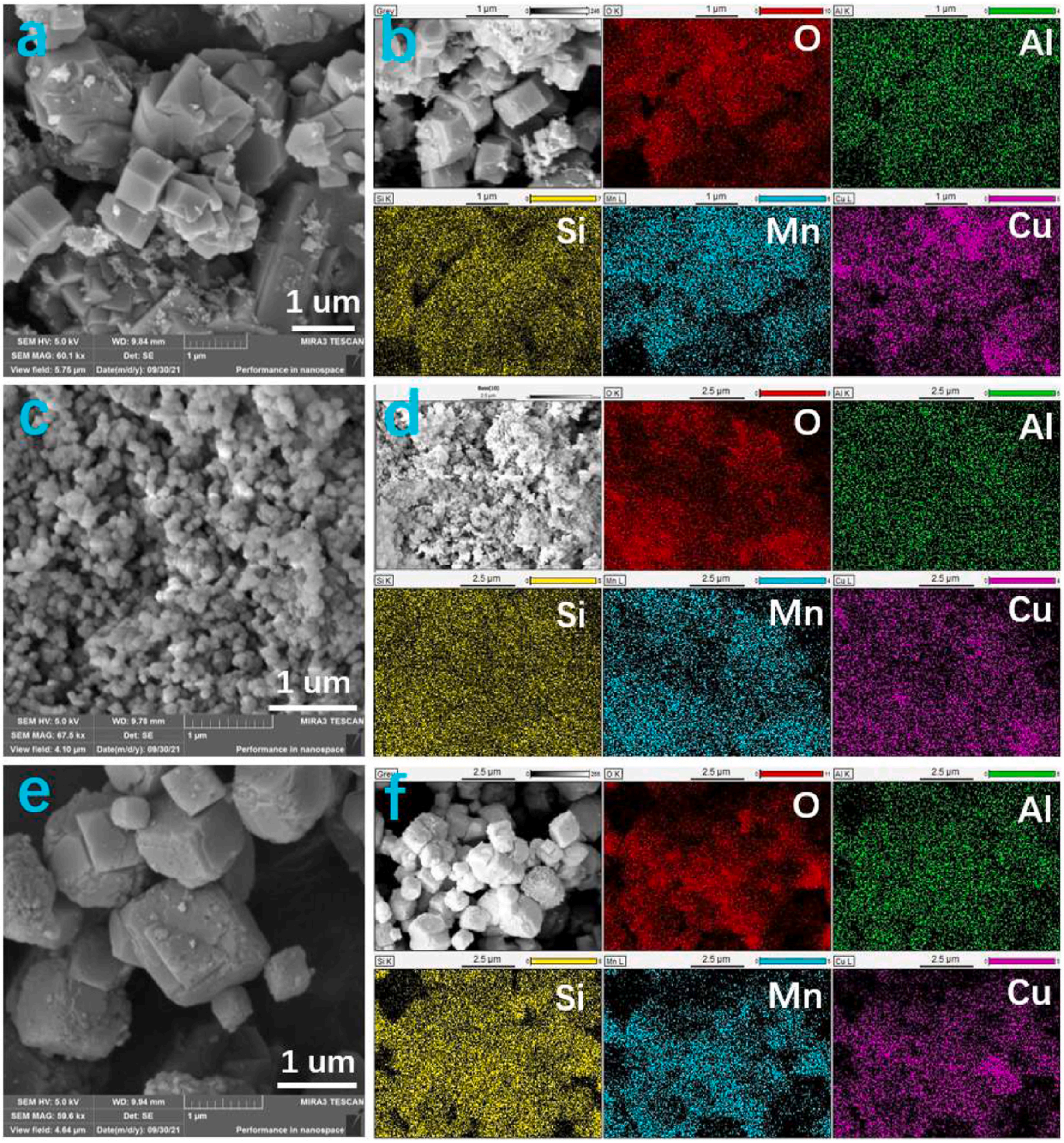

**Fig. 4.** SEM images and EDX mapping of (a) (b) CM/Z; (c) (d) CM/B; and (e) (f) CM/S.

1573 cm$^{-1}$, respectively [39]. Free dinitrogen trioxide produces products in two forms, *as*-$N_2O_3$ at 1300 cm$^{-1}$ and *s*-$N_2O_3$ at 1192, 1176 and 1030 cm$^{-1}$ [40]. Other form of oxides may also form in the gas phase, in particular $N_2O_4$ with vibrational bands at 1750 cm$^{-1}$ [41]. Each of the above species can be found in one or several surface coordination forms, bond to the zeolite lattice or to copper ions. The weak peak of adsorbed $N_2O$ disappears with the temperature increasing in Fig. 7(a). In general, $N_2O$ acts as an intermediate decomposes quickly at high temperatures and few parts of $N_2O$ still adsorb on the catalyst surface [42]. The intensity of peaks for adsorbed NO are strong at 30 °C and gradually disappear with the increase of temperature. At the same time, $NO_2^+$ and adsorbed $NO_2$ species are produced at 200 °C and then gradually decomposed at higher temperatures. Therefore, a catalytic effect of Cu species over CM/Z mainly promotes NO disproportionation to intermediate species of $N_2O$ and $NO_2$. After adding 2 vol% $O_2$ in Fig. 7(b), The intensity of adsorbed $N_2O$ (2207 cm$^{-1}$) and $NO_2$ species (2133 cm$^{-1}$) become stronger than that in 1 vol% NO/He, and quickly decomposes at higher temperatures, which indicates that the suitable amount of $O_2$ may promote the NO conversion. However, excess $O_2$ leads to formation of more nitrate species (1600 and 1573 cm$^{-1}$), free dinitrogen trioxide (1300 cm$^{-1}$) and $N_2O_4$ (1745 cm$^{-1}$) with higher intensity bands. In particular, the nitrate species become more stable and even retain at 500 °C although the similar variation occurs for other peaks. It can be informed that the $O_2$ facilitates the formation of stable nitrate species on the surface, restricting the activity of catalyst in some degree [43]. It should be noted that the intensity of adsorbed NO on Cu species is similar in Figs. 7(a) and 7(b), which demonstrates that the Cu species acts as the main active center, and the active intermediate species are probably $N_2O$ and $NO_2$ species instead of nitrate.

The labeled experiment ($^{18}O_2$) in the steady-state via transit switching was carried out to further understand the intrinsic effect of $O_2$ during NDD reaction, as shown in Fig. 8. The CM/Z was firstly pretreated in pure Ar at 550 °C. After switching the 1 vol% NO/Ar, the stable signals of $N_2$ and $^{16}O_2$ can be detected because of the effective NDD at 550 °C on the catalyst. The mixed gas of 1 vol% NO + 1 vol% $^{18}O_2$/Ar was then introduced into the reactor after purging with Ar

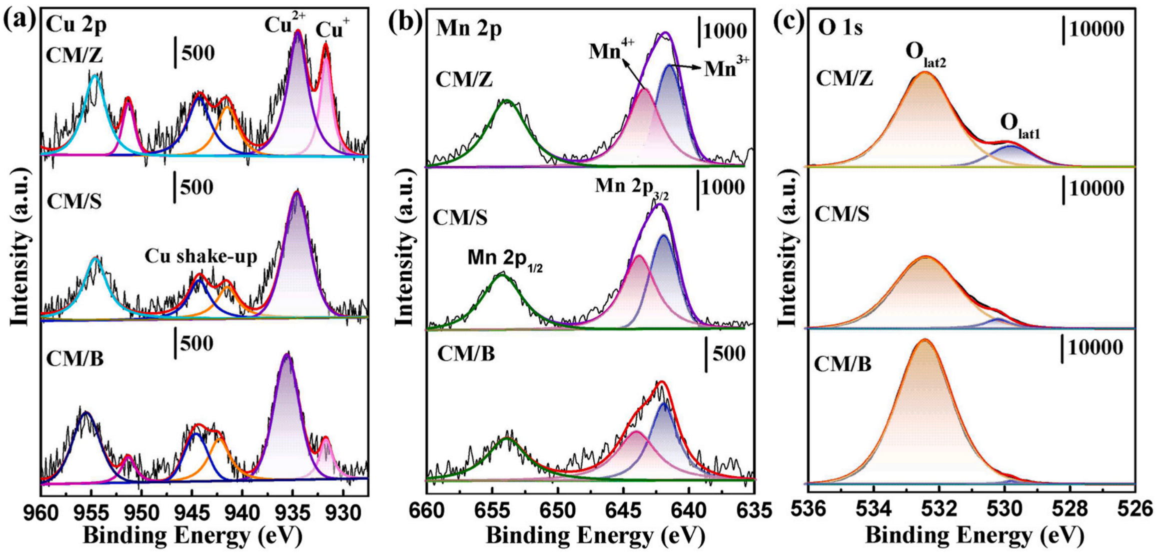

**Fig. 5.** XPS spectra (a) Cu 2p, (b) Mn 2p and (c) O 1 s of catalysts.

**Table 2**
The element ratios of the samples from XPS results.

| Sample | $Cu^+/Cu^{2+}$ | $Mn^{3+}/Mn^{4+}$ | $O_{lat1}/(O_{lat1}+O_{lat2})$ |
|---|---|---|---|
| CM/Z | 0.46 | 0.91 | 0.16 |
| CM/B | 0.18 | 1.04 | 0.01 |
| CM/S | 0.00 | 0.90 | 0.06 |

(30 mL/min). The stable signal of $N_2$ was observed, and the intensity of $N_2$ at 1 vol% NO + 1 vol% $^{18}O_2$/Ar is slightly weaker than that of 1 vol% NO/Ar, indicating that the addition of $O_2$ exhibits a moderate inhibition effect, in agreement with the results of activity. Here, three different $O_2$ isotopomer products ($^{16}O_2$, $^{16}O^{18}O$ and $^{18}O_2$) were found in turn. Firstly, large amounts of $^{16}O_2$ produced quickly, and then increased gradually with increasing the reaction time, attributed to NDD product, releasing from the catalyst itself. $N^{18}O$ should be considered to produce at the same time due to the same *m/z* (32) to $^{16}O_2$. The gradual increase of signal can be assigned to the $N^{18}O$, which is in consistency with the decreased signal of NO. It reflects that the oxygen of NO can be exchanged with the adsorbed $^{18}O$ from the catalyst surface to form $N^{18}O$, which is also reported by Damma et al. [44]. Afterwards, the cross-labeled $^{16}O^{18}O$ molecule generated quickly, implying that the suitable $^{18}O$ species adsorbed on the surface oxygen vacancies promotes the formation of $^{16}O^{18}O$. Finally, the signal of $^{18}O_2$ increased gradually and reached a steady state with the increase of reaction time, assigned to the excess gaseous $^{18}O_2$ fills into more oxygen vacancies firstly but cannot be exchange completely in NDD reaction, resulting in a competitive adsorption with NO on the oxygen vacancies and thus the catalytic activity decreases slightly. In addition, very small amounts of imtermediate apecies ($N_2^{16}O$, $N^{16}O^{18}O$ and $N^{16}O_2/N_2^{18}O$) were detected, which may not decopose.

## 4. Discussion

### 4.1. Support effect of catalyst

The intrinsic catalytic activity (NTN2) in Fig. 1 decreased in an order of CM/Z (53.4%) > CM/B (49.2%) > CM/S (7.9%) at 550 °C. The activity decreases from 53.4% to 40.3% at 550 °C after adding 1 vol% $O_2$ and maintains a good stability with 40% over 8 h on CM/Z catalyst sample, indicating the existence of $O_2$ produces a moderate inhibition effect. It remarks the significant effect of the support on the activity for NDD. The strong metal-support effect is evident on the CM/Z and CM/B whilst the weak interaction exists on CM/S. The CM/Z exhibits a better performance than the reported Cu-ZSM-5 samples in the references [38, 45]. The XRF results (Table 1) show the Si/Al ratios of CM/Z, CM/B and CM/S are 13.4, 13.5, and 9.3, respectively. It is reported that the higher silica-alumina ratio is beneficial to promote the activity in NDD, and the NTN2 at 500 °C is about 50% and 5% with Si/Al at 20 and 10, respectively [46]. The XRD (Fig. 2) and SEM+EDX (Fig. 4) results display that the Cu and Mn are well dispersed on the zeolite surface of all the samples, although the CM/S owns a larger specific BET surface area (Fig. 3). Furthermore, the XPS results in Fig. 5 reveal the higher ratio of $Cu^+/Cu^{2+}$ and $O_{lat1}/(O_{lat1}+O_{lat2})$ over the CM/Z, as compared to that in the CM/B and CM/S sample. Combined with $H_2$-TPR results (Fig. 6a), the higher amounts of active copper sites of $(Cu^{2+}\text{-}O^{2-}\text{-}Cu^{2+})^{2+}$ and $(Cu^+\text{-}\square\text{-}Cu^+)^{2+}$ dimers exist in CM/Z. The coexistence of copper and manganese improve the oxygen mobility at temperature region of activity, particularly for CM/Z, verified by $O_2$-TPD results (Fig. 6b). The addition of manganese is beneficial to improve the resistance of $O_2$. The reducibility and capacity of oxygen mobility follows the sequence of CM/Z > CM/B > CM/S, in consistency with the activity results. On the basis of NO-TPD results (Fig. 6c), The CM/Z shows the highest NO adsorption capacity with the largest amount of NO desorption (27.62 umol/g), which is in accordance to the large amount of $(Cu^{2+}\text{-}O^{2-}\text{-}Cu^{2+})^{2+}$ and $(Cu^+\text{-}\square\text{-}Cu^+)^{2+}$ sites. This suggests that the adsorbed NO can be generated and activated easily on the Cu-dimers dispersed on ZSM-5 [16]. Liu et al. found that the $(Cu^{2+}\text{-}O^{2-}\text{-}Cu^{2+})^{2+}$ dimers of La-Ni-Cu-ZSM-5 acted as the main active sites for NDD [18]. Hwak et al. revealed that the $NO^+$ species can also occupy cationic positions in close proximity of $Cu^+$ ions by forming $Cu^+\text{-}NO^+$ complexes to compensate negative zeolite framework charge, benefitting to strengthen the metal-support interaction [47].

### 4.2. Reaction mechanism

Supported by in situ DRIFT and the oxygen label experiment ($^{18}O_2$) results, the reaction mechanism of NDD over CM/Z is proposed as Eqs. (3)–(6) and shown in Fig. 9. In Eq. (3), two gaseous NO molecules are firstly adsorbed on the oxygen vacancy ($O_v$, $\square$) and Cu site of $(Cu^+\text{-}\square\text{-}Cu^+)^{2+}$ dimer to form $(Cu^{2+}\text{-}O^{2-}\text{-}Cu^{2+})^{2+}$ and $N_2O$. Eq. (4) shows that the $N_2O$ can be easily adsorbed on the oxygen vacancy of $(Cu^+\text{-}\square\text{-}Cu^+)^{2+}$ and activated to decompose into $N_2$ with oxygen transfer from $N_2O$ to $(Cu^{2+}\text{-}O^{2-}\text{-}Cu^{2+})^{2+}$. *In situ* DRIFT results evidenced that the intermediate $N_2O$ (Fig. 7a) is formed and decomposed quickly with the increase of temperature. Morpurgo [19] carried out a DFT examination

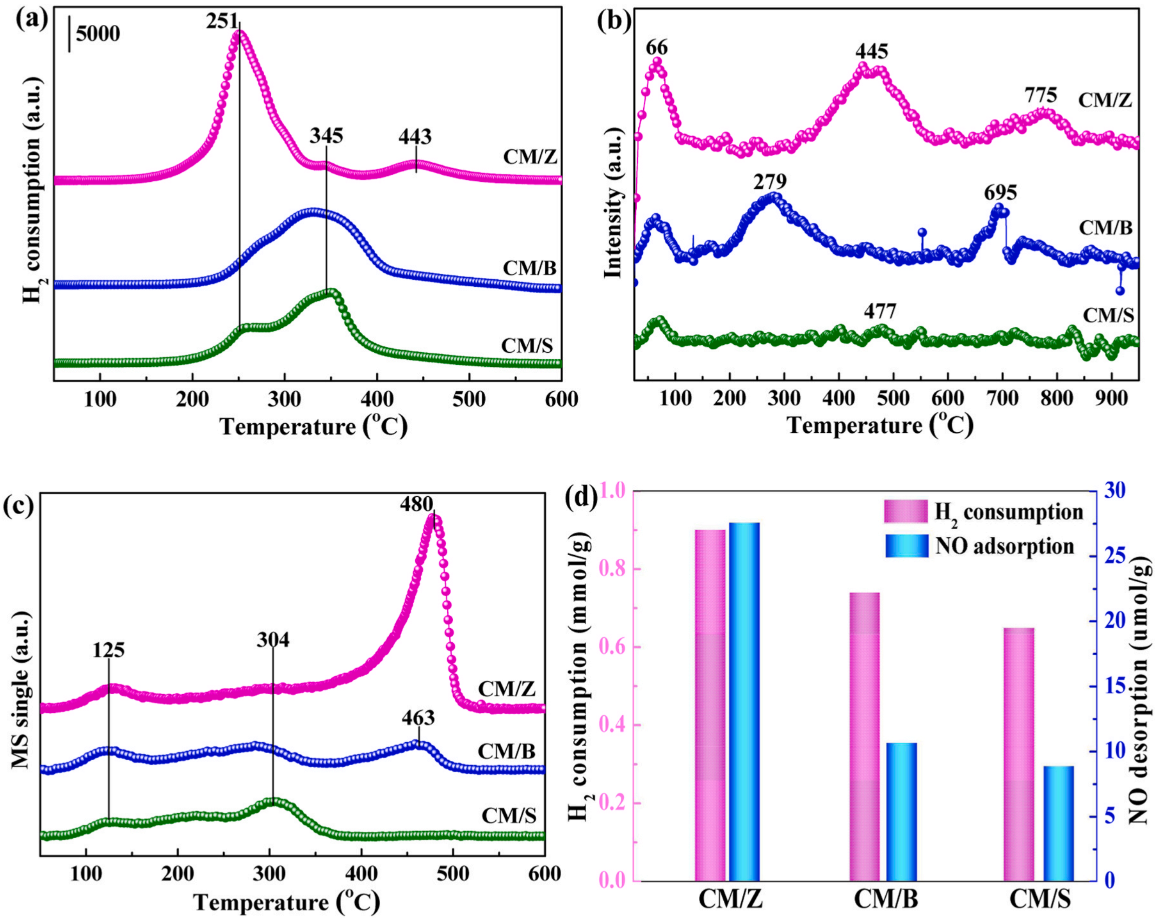

**Fig. 6.** (a) $H_2$-TPR, (b) $O_2$-TPD, (c) NO-TPD and (d) $H_2$ consumption and NO adsorption of catalysts.

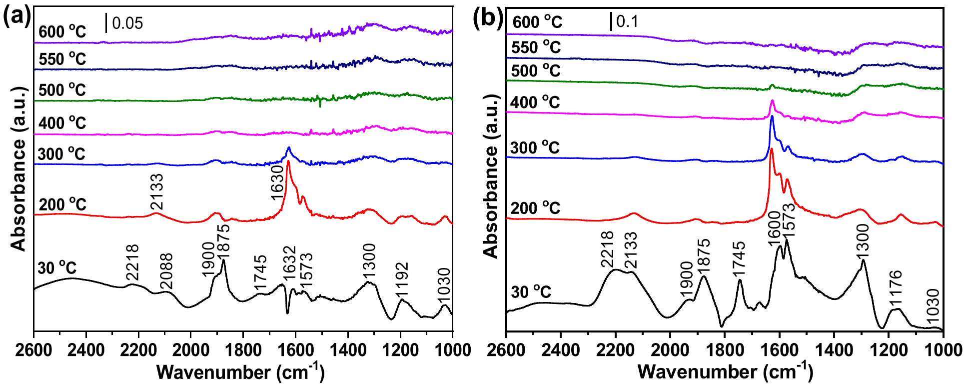

**Fig. 7.** *In situ* DRIFT spectra for (a) 1 vol%NO/He and (b) 1 vol%NO+ 2 vol%$O_2$/He over the CM/Z.

and verified that the best way for $N_2O$ intermediate to decompose is the direct, spin-forbidden reaction pathway on a reduced $Cu^{+}\ldots Cu^{+}$ pair on the Cu-ZSM-5, with the formation of $[Cu\text{-}O\text{-}Cu]^{2+}$ and $N_2$. The geometric and electronic structural criteria for binuclear CuI sites in Cu–ZSM-5 to activate $N_2O$ have been also found [20]. The transition pathway of the $(Cu^{2+}\text{-}O^{2-}\text{-}Cu^{2+})^{2+}$ to produce $(Cu^{+}\text{-}\square\text{-}Cu^{+})^{2+}$ dimer and release $O_2$ as a cycle for NDD can be approximately described via Eqs. (5) and (6). In Eq. (5), the gaseous NO is adsorbed on the $Cu^{2+}$ sites of $(Cu^{2+}\text{-}O^{2-}\text{-}Cu^{2+})^{2+}$ to form nitrite species $(Cu^{+}\text{-}NO_2\text{-}Cu^{+})^{2+}$. As revealed in the literature, NO can be adsorbed on $Cu^{2+}$ to form $Cu^{+}\text{-}NO^{+}$ via the reduction of $Cu^{2+}$ [47,48]. Subsequently, this unstable transition species decomposes to form $(Cu^{+}\text{-}\square\text{-}Cu^{+})^{2+}$ with oxygen vacancy and $NO_2$. The dimer $(Cu^{2+}\text{-}O^{2-}\text{-}Cu^{2+})^{2+}$ adsorbs $NO_2$ to form nitrate species, and further decomposes into $(Cu^{+}\text{-}\square\text{-}Cu^{+})^{2+}$, NO and $O_2$ in Eq. (6), in agreement with the in situ DRIFT results of the decomposition of nitrite and nitrate species at high temperature. Thus, the dimers including $(Cu^{+}\text{-}\square\text{-}Cu^{+})^{2+}$ and $(Cu^{2+}\text{-}O^{2-}\text{-}Cu^{2+})^{2+}$ act as main active sites with a redox cycle over CM/Z to form primary intermediate species of $N_2O$ and $NO_2$, respectively, for NDD. The added $O_2$ is probably adsorbed on oxygen vacancy of dimers and exchanged with the oxygen from the CM/Z catalyst and/or NO to desorb $O_2$, verified by the oxygen label experiment ($^{18}O_2$) results (Fig. 8). This competitive adsorption between NO and $O_2$ over CM/Z is the main reason for $O_2$ inhibition.

$$(Cu^{+}\text{-}\square\text{-}Cu^{+})^{2+} + 2NO \rightarrow (Cu^{2+}\text{-}O^{2-}\text{-}Cu^{2+})^{2+} + N_2O \quad (3)$$

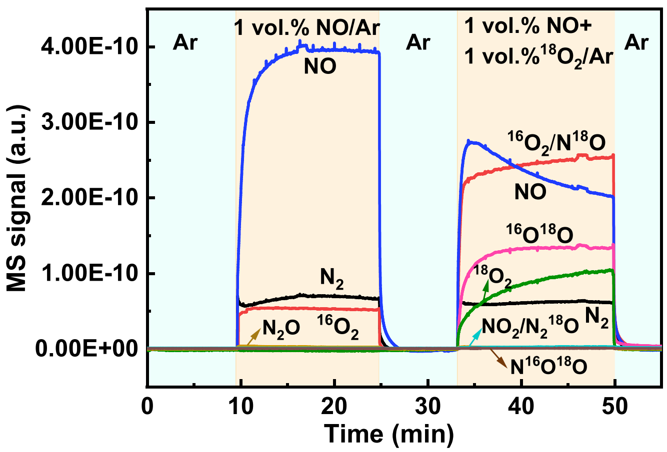

**Fig. 8.** Isotopic ($^{18}O_2$) exchange experiments at 550 °C over CM/Z.

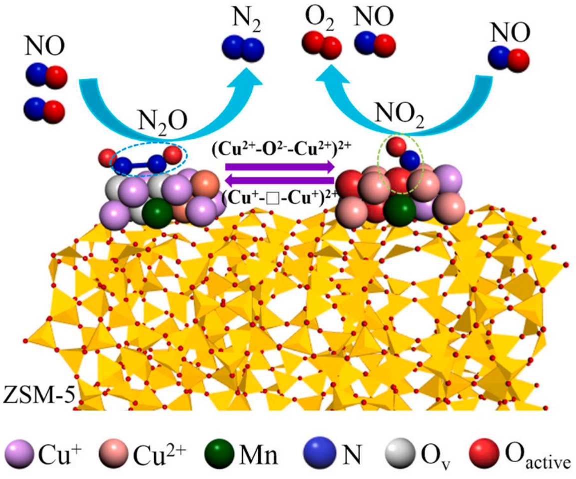

**Fig. 9.** The proposed reaction pathways in NO direct decomposition over CM/Z.

$$(Cu^{+}\text{-}\square\text{-}Cu^{+})^{2+} + N_2O \rightarrow (Cu^{2+}\text{-}O^{2-}\text{-}Cu^{2+})^{2+} + N_2 \tag{4}$$

$$(Cu^{2+}\text{-}O^{2-}\text{-}Cu^{2+})^{2+} + NO \rightarrow (Cu^{+}\text{-}\square\text{-}Cu^{+})^{2+} + NO_2 \tag{5}$$

$$(Cu^{2+}\text{-}O^{2-}\text{-}Cu^{2+})^{2+} + NO_2 \rightarrow (Cu^{+}\text{-}\square\text{-}Cu^{+})^{2+} + NO + O_2 \tag{6}$$

## 5. Conclusion

The catalytic activity for NO direct decomposition decreases in the order of CM/Z (53.4%) > CM/B (49.2%) > CM/S (7.9%) at 550 °C. On CM/Z with adding 1 vol% $O_2$, the conversion decreases from 53.4% to 40.3% at 550 °C and keeps a good stability with 40% for 8 h. The competitive adsorption between NO and $O_2$ on the oxygen vacancy of dimers over CM/Z results in the activity decrease after adding $O_2$. The excellent activity obtained with CM/Z is attributed to the strong metal-support interaction including suitable ratio of Si/Al, forming more active copper sites of the $(Cu^{2+}\text{-}O^{2-}\text{-}Cu^{2+})^{2+}$ and $(Cu^{+}\text{-}\square\text{-}Cu^{+})^{2+}$ dimers, which have high redox activity, capacity of oxygen mobility, and NO sorption capability. The copper species acts as the main active site and the addition of manganese is beneficial to improve the resistance of $O_2$ on CM/Z. The reaction pathway involves two NO adsorbs on $(Cu^{+}\text{-}\square\text{-}Cu^{+})^{2+}$ to form $N_2O$, then $N_2O$ is activated to produce $N_2$ and $(Cu^{2+}\text{-}O^{2-}\text{-}Cu^{2+})^{2+}$, followed by the NO adsorption on $(Cu^{2+}\text{-}O^{2-}\text{-}Cu^{2+})^{2+}$ to form nitrite and nitrate species and decompose into NO, $O_2$ and $(Cu^{+}\text{-}\square\text{-}Cu^{+})^{2+}$.

## CRediT authorship contribution statement

**Bin Feng:** Writing – review & editing, Supervision, Methodology, Formal analysis. **Li Yongdan:** Writing – review & editing, Resources, Methodology, Funding acquisition, Conceptualization. **Chen Hong:** Writing – review & editing, Methodology, Formal analysis. **Zhang Cuijuan:** Writing – review & editing, Formal analysis. **Wang Gang:** Writing – review & editing, Resources, Formal analysis. **An Sufeng:** Resources, Investigation. **Wang Xuehai:** Writing – review & editing, Resources, Formal analysis. **Kang Running:** Writing – original draft, Investigation, Data curation, Conceptualization.

## Declaration of Competing Interest

The authors declare that they have no known competing financial interests or personal relationships that could have appeared to influence the work reported in this paper.

## Data availability

Data will be made available on request.

## Acknowledgements

The authors gratefully acknowledge the financial support from the International Science and Technology Cooperation Projects (Sinopec. 410920). R. Kang sincerely acknowledge the financial support from the China Scholarship Council (CSC, No. 202004910623).

## References

[1] H. Zhao, X. Chen, A. Bhat, Y. Li, J.W. Schwank, Understanding the chemistry during the preparation of Pd/SSZ-13 for the low-temperature NO adsorption: The role of NH4-SSZ-13 support, Appl. Catal. B: Environ. 282 (2021) 119611.

[2] J. Wang, H. Chen, Z. Hu, M. Yao, Y. Li, A review on the Pd-based three-way catalyst, Catal. Rev. Sci. Eng. 57 (2015) 79–144.

[3] R. Kang, J. He, F. Bin, B. Dou, Q. Hao, X. Wei, K. Hui, K.S. Hui, Alkali metal-resistant mechanism for selective catalytic reduction of nitric oxide over $V_2O_5$/HWO catalysts, Fuel 304 (2021) 121445.

[4] J. Wang, H. Zhao, G. Haller, Y. Li, Recent advances in the selective catalytic reduction of $NO_x$ with $NH_3$ on Cu-Chabazite catalysts, Appl. Catal. B: Environ. 202 (2017) 346–354.

[5] Y. Yang, J. Liu, F. Liu, Z. Wang, J. Ding, H. Huang, Reaction mechanism for $NH_3$-SCR of $NO_x$ over $CuMn_2O_4$ catalyst, Chem. Eng. J. 316 (2019) 578–587.

[6] V.I. Pârvulescu, P. Grange, B. Delmon, Catalytic removal of NO, Catal. Today 46 (1998) 233–316.

[7] L. Zhang, D. Wang, Y. Liu, K. Kamasamudram, J. Li, W. Epling, $SO_2$ poisoning impact on the $NH_3$-SCR reaction over a commercial Cu-SAPO-34 SCR catalyst, Appl. Catal. B: Environ. 156–157 (2014) 371–377.

[8] Y. Zhang, G. Cao, X. Yang, Advances in De-$NO_x$ methods and catalysts for direct catalytic decomposition of NO: A review, Energy Fuels 35 (2021) 6443–6464.

[9] F. Garin, Mechanism of $NO_x$ decomposition, Appl. Catal. A. Gen. 222 (2001) 183–219.

[10] P. Xie, W.X. Ji, Y. Li, C. Zhang, NO direct decomposition: progress, challenges and opportunities, Catal. Sci. Technol. 11 (2021) 374–391.

[11] H.R. Wang, X.C. Li, F.R. Meng, G.Y. Wang, D.K. Zhang, Preparation and evaluation of iron nanoparticles embedded CNTs grown on ZSM-5 as catalysts for NO decomposition, Chem. Eng. J. 392 (2020) 123798.

[12] Y.Y. Zhang, G.J. Cao, X. Yang, Advances in De-NOx methods and catalysts for direct catalytic decomposition of NO: A Review, Energy Fuels 35 (2021) 6443–6464.

[13] A. Fritz, V. Pitchon, The current state of research on automotive lean $NO_x$ catalysis, Appl. Catal., B: Environ. 13 (1997) 1–25.

[14] M. Iwamoto, H. Furukawa, Y. Mine, F. Uemura, S. Mikuriya, S. Kagawa, Copper (II) ion-exchanged ZSM-5 zeolites as highly active catalysts for direct and continuous decomposition of nitrogen monoxide, J. Chem. Soc., Chem. Commun. (16) (1986) 1272–1273.

[15] M. Iwamoto, H. Yahiro, Novel catalytic decomposition and reduction of NO, Catal. Today 22 (1994) 5–18.

[16] X.F. Wang, X. Yang, X.L. Qiao, J.N. Guo, J.R. Guo, Y. Jin, B.G. Fan, Effect of water vapor on catalytic decomposition of NO over Cu−ZSM-5: A mechanism and kinetic study, Energy Fuels 34 (2020) 11341–11352.

[17] V. Pârvulescu, P. Grange, B. Delmon, NO decomposition over physical mixtures of Cu-ZSM-5 with zeolites or oxides, Appl. Catal. B: Environ. 33 (2001) 223–237.

[18] M.K. Liu, Y.N. Zhao, H.W. Zhao, X.H. Li, Y.H. Ma, X. Yong, H. Chen, Y.D. Li, The promotion effect of nickel and lanthanum on Cu-ZSM-5 catalyst in NO direct decomposition, Catal. Today 327 (2019) 203–209.

[19] S. Morpurgo, A DFT study on the mechanism of NO decomposition catalyzed by short-distance Cu(I) pairs in Cu-ZSM-5, Mol. Catal. 434 (2017) 96–105.

[20] M.L. Tsai, R.G. Hadt, P. Vanelderen, B.F. Sels, R.A. Schoonheydt, E.I. Solomon, $[Cu_2O]^{2+}$ active site formation in Cu–ZSM-5: geometric and electronic structure requirements for $N_2O$ activation, J. Am. Chem. Soc. 136 (2014) 3522–3529.

[21] Y.H. Ma, H.W. Zhao, C.J. Zhang, Y.N. Zhao, H. Chen, Y.D. Li, Enhanced hydrothermal stability of Cu-SSZ-13 by compositing with Cu-SAPO-34 in selective catalytic reduction of nitrogen oxides with ammonia, Catal. Today 355 (2020) 627–634.

[22] S. Brandenberger, O. Kröcher, A. Wokaun, A. Tissler, R. Althoff, The role of Brønsted acidity in the selective catalytic reduction of NO with ammonia over Fe-ZSM-5, J. Catal. 268 (2009) 297–306.

[23] T. Wang, X.Y. Zhang, J. Liu, Y. Wang, B.M. Sun, Effects of temperature on $NO_x$ removal with Mn-Cu/ZSM5 catalysts assisted by plasma, Appl. Therm. Eng. 130 (2018) 1224–1232.

[24] H.R. Lei, D.D. Chen, J.Y. Yang, A. Khetan, J.X. Jiang, B.X. Peng, U. Simon, D.Q. Ye, P.R. Chen, Revealing the formation and reactivity of cage-confined Cu pairs in catalytic $NO_x$ reduction over Cu-SSZ-13 zeolites by in situ UV−Vis spectroscopy and time-dependent DFT calculation, Environ. Sci. Technol. 57 (2023) 12465–12475.

[25] R.N. Kang, J.Q. Huang, F. Bin, Z.H. Teng, X.L. Wei, B.J. Dou, S. Kasipandi, Evolution behavior and active oxygen quantification of reaction mechanism on cube $Cu_2O$ for CO self-sustained catalytic combustion and chemical-looping combustion, Appl. Catal. B: Environ. 310 (2022) 121296.

[26] B. Ganemi, E. Björnbom, B. Demirel, J. Paul, Zeolite Cu–ZSM-5: material characteristics and NO decomposition, Microporous Mesoporous Mater. 38 (2000) 287–300.

[27] M.R. Apelian, A.S. Fung, G.J. Kennedy, T.F. Degnan, Dealumination of zeolite β via dicarboxylic acid treatment, J. Phys. Chem. 100 (1996) 16577–16583.

[28] F. Bin, C. Song, G. Lv, J. Song, S. Wu, X. Li, Selective catalytic reduction of nitric oxide with ammonia over zirconium-doped copper/ZSM-5 catalysts, Appl. Catal. B: Environ. 150-151 (2014) 532–543.

[29] C. He, Y.K. Yu, L. Yue, N.L. Qiao, J.J. Li, Q. Shen, W.J. Yu, J.S. Chen, Z.P. Hao, Low-temperature removal of toluene and propanal over highly active mesoporous CuCeOx catalysts synthesized via a simple self-precipitation protocol, Appl. Catal. B: Environ. 147 (2014) 156–166.

[30] N. Katabathini, H.A.E.M. Islam, M. Mohamed, Cu, Fe and Mn oxides intercalated $SiO_2$ pillared magadiite and ilerite catalysts for NO decomposition, Appl. Catal. A: Gen. 616 (2021) 118110.

[31] Y. Du, M.S. Zhang, J. Hong, Y. Shen, Q. Chen, Z. Yin, Structural and optical properties of nanophase zinc oxide, Appl. Phys. A. 76 (2003) 171–176.

[32] C. Torre-Abreu, M.F. Ribeiro, C. Henriques, G. Delahay, Characterisation of CuMFI catalysts by temperature programmed desorption of NO and temperature programmed reduction. Effect of the zeolite Si/Al ratio and copper loading, Appl. Catal. B: Environ. 12 (1997) 249–262.

[33] Y. Teraoka, C. Tai, H. Ogawa, H. Furukawa, S. Kagawa, Characterization and NO decomposition activity of Cu-MFI zeolite in relation to redox behavior, Appl. Catal. A: Gen. 200 (2000) 167–176.

[34] C. Liu, R.N. Kang, F. Bin, X.L. Wei, K.N. Hui, S. Kasipandi, K.S. Hui, Insights on copper, manganese, and Nickel/ZSM-5 catalytic mechanisms for nitric oxides selective reduction with ammonia, Carbon Resour. Convers. 5 (2022) 15–25.

[35] L. Zhu, J. Yu, X. Wang, Oxidation treatment of diesel soot particulate on $Ce_xZr_{1-x}O_2$, J. Hazard. Mater. 140 (1-2) (2007) 205–210.

[36] C. Torre-Abreu, M.F. Ribeiro, C. Henriques, G. Delahay, Characterisation of CuMFI catalysts by temperature programmed desorption of NO and temperature programmed reduction. Effect of the zeolite Si/Al ratio and copper loading, Appl. Catal. B: Environ. 12 (1997) 249–262.

[37] P.J. Smeets, M.H. Groothaert, R.M. Teeffelen, H. Leeman, E.J.M. Hensen, R. A. Schoonheydt, Direct NO and $N_2O$ decomposition and NO-assisted $N_2O$ decomposition over Cu-zeolites: Elucidating the influence of the Cu–Cu distance on oxygen migration, J. Catal. 245 (2007) 358–368.

[38] B. Ganemi, E. BjÖrnbom, J. Paul, Conversion and in situ FTIR studies of direct NO decomposition over Cu-ZSM5, Appl. Catal. B Environ. 17 (1998) 293–311.

[39] D. Pozdnyakov, V. Filimonov, Infrared spectroscopic study of the chemisorption of nitric oxide and nitrogen dioxide on metal oxides, Kinet. Katal. 14 (1973) 760–766.

[40] E.M. Nour, L.H. Chen, J. Laane, Interconversion studies and characterization of asymmetric and symmetric dinitrogen trioxide in nitric oxide matrixes by Raman and infrared spectroscopy, J. Phys. Chem. 87 (1983) 1113–1120.

[41] C.Y. Lee, K.Y. Choi, B.H. Ha, Catalytic decomposition of nitric oxide on copper/zeolites, Appl. Catal. B Environ. 5 (1994) 7–21.

[42] T. Ishihara, M. Ando, K. Sada, K. Takiishi, K. Yamada, H. Nishiguchi, Y. Takita, Direct decomposition of NO into $N_2$ and $O_2$ over La(Ba)Mn(In)$O_3$ perovskite oxide, J. Catal. 220 (2003) 104–114.

[43] S. Xie, M.P. Rosynek, J.H. Lunsford, Catalytic reactions of NO over 0–7 mol% Ba/MgO catalysts: I. the direct decomposition of NO, J. Catal. 188 (1999) 24–31.

[44] D. Damma, T. Boningari, P.R. Ettireddy, B.M. Reddy, P.G. Smirniotis, Direct decomposition of $NO_x$ over $TiO_2$ supported transition metal oxides at low temperatures, Ind. Eng. Chem. Res. 57 (2018) 16615–16621.

[45] T. Ohnishi, K. Kawakami, M. Nishioka, M. Ogura, Direct decomposition of NO on metal-loaded zeolites withcoexistence of oxygen and water vapor under unsteady-stateconditions by NO concentration and microwave rapid heating, Catal. Today 281 (2017) 566–574.

[46] Y.L. Gan, S.P. Cui, X.Y. Ma, Y.L. Wang, Effect of silica-alumina ratio of catalysts on NO decomposition rate in cement kiln exhaust, Mater. Sci. Forum 993 (2020) 1450–1455.

[47] J.H. Kwak, J.H. Lee, S.D. Burton, A.S. Lipton, C.H.F. Peden, J. Szanyi, A common intermediate for $N_2$ formation in enzymes and zeolites: side-on Cu–nitrosyl complexes, Angew. Chem., Int. Ed. 52 (2013) 9985–9989.

[48] D.D. Chen, Y.L. Yan, A.Q. Guo, V. Rizzotto, H.R. Lei, Z.W. Qiao, H. Liang, M. Jabłońska, X.Q. Jiang, J.X. Jiang, R. Palkovits, P.R. Chen, D.Q. Ye, U. Simon, Mechanistic insights into the promotion of low-temperature $NH_3$-SCR catalysis by copper auto-reduction in Cu-zeolites, Appl. Catal. B: Environ. 322 (2023) 122118.